

TESTING THE NATURE OF THE SUPERMASSIVE BLACK HOLE CANDIDATE IN SgrA* WITH LIGHT CURVES AND IMAGES OF HOT SPOTS

ZILONG LI, LINGYAO KONG, AND COSIMO BAMBI^a

Center for Field Theory and Particle Physics & Department of Physics, Fudan University, 200433 Shanghai, China

Draft version October 15, 2018

ABSTRACT

General relativity makes clear predictions about the spacetime geometry around black holes. In the near future, new facilities will have the capability to explore the metric around SgrA*, the supermassive black hole candidate at the Center of our Galaxy, and open a new window to test the Kerr black hole hypothesis. In this paper, we compute light curves and images associated with compact emission regions (hot spots) orbiting around Kerr and non-Kerr black holes. We study how the analysis of the properties of the radiation emitted by a hot spot can be used to test the Kerr nature of SgrA*. We find that the sole observation of the hot spot light curve can at most constrain a combination of the black hole spin and of possible deviations from the Kerr solution. This happens because the same orbital frequency around a Kerr black hole can be found for a non-Kerr object with a different spin parameter. Second order corrections in the light curve due to the background geometry are typically too small to be identified. While the observation of the hot spot centroid track can potentially bound possible deviations from the Kerr solution, that is out of reach for the near future VLTI instrument GRAVITY. The Kerr black hole hypothesis could really be tested in the case of the discovery of a radio pulsar in a compact orbit around SgrA*. Radio observations of such a pulsar would provide precise estimates of the mass and the spin of SgrA*, and the combination of these measurements (probing the weak field) with the hot spot light curve information (probing the strong field) may constrain/find possible deviations from the Kerr solution with quite good precision.

Subject headings: black hole physics — Galaxy: center — gravitation

1. INTRODUCTION

In 4-dimensional general relativity, uncharged black holes (BHs) are described by the Kerr solution and are completely characterized by only two quantities: the mass M and the spin parameter $a = J/M$, where J is the BH spin angular momentum. Astrophysical BH candidates are thought to be the Kerr BHs predicted in general relativity simply because they cannot be explained otherwise without introducing new physics. Stellar-mass BH candidates in X-ray binary systems have a mass of $M \approx 5 - 20 M_{\odot}$, which is too high for a neutron or quark star for any plausible matter equation of state (Rhoades & Ruffini 1974; Kalogera & Baym 1996). At least some supermassive BH candidates at the center of galaxies are definitively too massive, compact, and old to be a cluster of compact non-luminous objects, as the cluster lifetime due to evaporation and physical collisions would be shorter than the age of these systems (Maoz 1998). The non-observation of electromagnetic radiation emitted by the possible surface of these objects may also be interpreted as an evidence for the presence of an event horizon (Narayan & Heyl 2002; Narayan & McClintock 2008; Broderick et al. 2009), but only if we exclude the possibility of new physics (Abramowicz et al. 2002; Bambi 2013e; Bambi et al. 2013). Despite these arguments, there is no direct indication that the spacetime geometry around BH candidates is described by the Kerr metric and so far the predictions of general relativity have been tested only in the weak field regime, while the validity of the theory in strong gravitational fields is totally unexplored.

In the last few years, the possibility of testing the Kerr nature of BH candidates by studying the properties of the electromagnetic radiation emitted by the gas in the accretion disk has been discussed by several authors and it has become a quite active line of research [for a review, see e.g. Bambi (2011b, 2013b)]. In this context, it is important to bear in mind two fundamental points, which instead are usually not well understood. First, strictly speaking the electromagnetic radiation emitted from the accretion disk can only be used to check if the spacetime geometry around BH candidates is described by the Kerr metric, not to test the validity of the Einstein equations. Indeed, these photons simply follow the null geodesics of the spacetime, independently of the exact equations determining the background metric. The Kerr metric is a solution of the Einstein equations, but it is common to other theories of gravity (Psaltis et al. 2008). If we want to test the validity of the Einstein equations, we should study the perturbations around this metric (Barausse & Sotiriou 2008). Second, contrary to common statements in the literature concerning tests of gravity in the strong field regime, the observation of features associated to relativistic effects absent in Newtonian gravity is not enough to test the Kerr BH hypothesis. The correct approach is instead to compare observational data with theoretical predictions in Kerr and non-Kerr backgrounds and see if the observations can distinguish the two scenarios. That is usually not the case, because there is a degeneracy between the spin and possible deviations from the Kerr metric, and a non-Kerr object looks like a Kerr BH with a different spin.

At present, there are two relatively robust techniques to probe the spacetime geometry around BH candidates and

^a Corresponding author: bambi@fudan.edu.cn

constrain possible deviations from the Kerr solution; that is, the fit of the thermal spectrum of thin disks (Zhang et al. 1997; Bambi & Barausse 2011; Bambi 2012e) and the analysis of the $K\alpha$ iron line profile (Fabian et al. 1989; Johannsen & Psaltis 2013; Bambi 2013a). However, it turns out that it is very difficult to test the Kerr BH paradigm, because often a non-Kerr BH looks like a Kerr one with a different spin. The disk’s thermal spectrum and the iron line profile can currently be used to exclude some exotic BH alternatives, like some wormholes (Bambi 2013c) and some exotic compact objects without event horizon (Bambi & Malafarina 2013; Joshi et al. 2014). More realistic scenarios can be extremely difficult to test (Bambi 2013f). Some tentative bounds inferred from current data are reported, for instance, in Bambi (2011a, 2014a,b) and Li & Bambi (2013).

In addition to the analysis of the disk’s thermal spectrum and of the iron line profile, there are some quite promising techniques for the future, especially if used in combinations with other measurements. For instance, the observed quasi-periodic oscillations (QPOs) in the X-ray flux of stellar-mass BH candidates may be a very powerful tool to probe the spacetime geometry around these objects (Johannsen & Psaltis 2011a; Bambi 2012d, 2013g). At present, the exact mechanism responsible for these phenomena is not understood and different scenarios provide different results, which makes it not yet possible to use QPOs to test fundamental physics. The same problem affects the measurements via the estimate of the jet power (Narayan & McClintock 2012; Bambi 2012b,c; McClintock et al. 2013): different models lead to different conclusions and at present we do not know which one is correct. In the future, it will be possible to test the nature of astrophysical BH candidates with data not yet available, like the polarization of X-ray radiation from the accretion disk (Krawczynski 2012) and pulsar timing (Wex & Kopeikin 1999; Liu et al. 2012).

A promising object to test the Kerr BH paradigm is SgrA*, the supermassive BH candidate at the Center of our Galaxy. For instance, very long baseline interferometry (VLBI) observations at mm wavelengths have recently shown that it will be probably possible to image the accretion flow around SgrA* within about 5 years (Doeleman et al. 2008, 2009) and open a new window to test general relativity in the strong field regime. The main goal of the Event Horizon Telescope¹ is the observation of the BH “shadow”, a dark area over a brighter background (Falcke et al. 2000; Takahashi 2004). While the intensity map of the image of the accretion flow depends also on complicated astrophysical processes, the exact shape of the shadow is only determined by the background geometry. Indeed, the boundary of the shadow corresponds to the apparent photon capture sphere of the background metric as seen by a distant observer. Starting from Bambi & Freese (2009) and Bambi et al. (2010), the shape of the shadow has been extensively studied to test the metric around SgrA* with future VLBI observations (Bambi & Yoshida 2010; Amarilla et al. 2010; Johannsen & Psaltis 2010; Bambi et al. 2012; Amarilla & Eiroa 2012; Bambi 2013d; Abdujabbarov et al. 2013; Amarilla & Eiroa 2013; Wei & Liu 2013; Li & Bambi 2014; Tsukamoto et al. 2014). For a review on the subject, see e.g. Falcke & Markoff (2013).

While the detection of the BH shadow is surely an extremely intriguing goal, tests of general relativity will probably require quite high resolutions, not available soon [but see Bambi (2013d)]. In the near future, a more promising possibility could be the observation of compact emission regions (hot spots) orbiting near the innermost stable circular orbit (ISCO) of SgrA*. Indeed, the latter exhibits powerful flares in the X-ray, NIR, and sub-mm bands (Genzel et al. 2003; Ghez et al. 2004; Eckart et al. 2004, 2009; Dodds-Eden et al. 2010, 2011; Trap et al. 2011); for a review, see e.g. Genzel et al. (2010). During the flares, the flux increases up to a factor 10. A flare typically lasts 1-3 hours and the rate is of a few events per day. Flares seem to show a quasi-periodic substructure with a time scale of about 20 minutes, but the presence of this substructure is still the subject of intense debate and some authors argue that it is not present in the data (Do et al. 2009). Several mechanisms have been proposed to explain these flares, such as the heating of electrons in a jet (Markoff et al. 2001), the adiabatic expansion of a blob of plasma (Yusef-Zadeh et al. 2006), Rossby wave instability in the disk (Tagger & Melia 2006), and blobs of plasma orbiting the ISCO of SgrA* (Hamaus et al. 2009). In this paper, we will assume that the last scenario of a hot spot near the ISCO is the correct one, but at present there is no reason to favor it. The hot spot model will be tested by the GRAVITY instrument for the ESO Very Large Telescope Interferometer (VLTI) (Eisenhauer et al. 2008, 2011; Vincent et al. 2011)².

Computations of images and light curves of hot spots in the Kerr metric for different values of the BH spin parameter, orbital radius, and viewing angle were previously reported in Schnittman & Bertschinger (2004), Schnittman (2005, 2006), Broderick & Loeb (2005, 2006), and Hamaus et al. (2009), where it has been shown that the mass and the spin of the BH may be extracted from their signatures in the flux and in the polarization of the hot spot. The aim of the present paper is to extend the study of a hot spot in a Kerr background to test the spacetime geometry around SgrA*. We compute images and light curves of an optically thick emitting disk orbiting around Kerr and non-Kerr BHs for different values of the model parameters. In particular, we want to see if it is possible to estimate the value of the spin and constrain deviations from the Kerr metric at the same time. As in the case of other approaches, it turns out that this is quite a difficult job. If we assume that the BH is of the Kerr type, the only parameter of the background geometry affecting the strong field regime is the spin (the mass can be inferred by dynamical methods, by studying the orbital motion of individual stars in the Newtonian regime). Any observable quantity that is a monotonic function of the spin can be used to infer the latter. If we relax the Kerr BH hypothesis, the properties of the spacetime metric close to the compact object depend on the spin as well as on possible deformations from the Kerr geometry. If the hot spot is orbiting at the ISCO, its light curve essentially tells us the ISCO frequency. While in the Kerr metric there is a one-to-one correspondence between BH spin and ISCO frequency (if the BH mass is known), that is not true any more in a non-Kerr background, because the ISCO frequency now depends also on the deformation parameter. The latter introduces also some small corrections to the shape of the light curve, but these corrections are

¹ URL: <http://www.eventhorizontelescope.org/>

² URL: <http://www.mpe.mpg.de/ir/gravity>

very small and they can unlikely be used to estimate the BH spin and the deformation parameter at the same time. The sole observation of the light curve of a hot spot orbiting at the ISCO can only select the spacetimes with the same ISCO frequency. The observation of the centroid track may distinguish spacetimes with the same ISCO frequency and thus constrain possible deviations from the Kerr solution, but a $10 \mu\text{s}$ precision like GRAVITY is not enough to do it. We find that an interesting possibility is the combination of the light curve information with the possible future observation of a pulsar orbiting SgrA* with a period of a few months. Such a pulsar would allow very precise measurements of the BH mass and spin (independently of the nature of the BH candidate, because it is relatively far from the compact object) (Liu et al. 2012). Once the mass and the spin are known, the ISCO frequency depends only on possible deviations from the Kerr solution. While the pulsar data might also independently constrain the BH quadrupole moment, a hot spot would provide more stringent constraints on the Kerr geometry, because it does not require that the BH spin is high and it is sensitive even to deviations of higher order.

The content of the paper is as follows. In Section 2, we review the calculations of images and light curves of hot spots in a Kerr background. In Section 3, we apply this approach to the case of non-Kerr spacetimes. In Section 4, we compare the observational properties of hot spots orbiting around Kerr and non-Kerr BHs to figure out how future observations can test the Kerr metric around SgrA*. Summary and conclusions are reported in Section 5. Throughout the paper, we use units in which $G_N = c = 1$.

2. HOT SPOTS ORBITING KERR BLACK HOLES

General relativistic magneto-hydrodynamic simulations of accretion flows onto BHs indicate that temporary clumps of matter may be common in the region near the ISCO (De Villiers et al. 2003; Schnittman et al. 2006). In the case of SgrA*, such a possibility seems to be supported by the observation of flaring activity in the X-ray, NIR, and sub-mm bands with a timescale of order the orbital frequency at the ISCO radius (Genzel et al. 2003; Ghez et al. 2004; Eckart et al. 2004, 2009; Dodds-Eden et al. 2010, 2011; Trap et al. 2011). A similar evidence comes from the X-ray spectrum of stellar-mass BH candidates in binary systems, where the observed QPOs in the X-ray flux have a frequency comparable to the expected fundamental orbital frequencies of a test-particle orbiting near the ISCO radius (Stella & Vietri 1998, 1999). All these arguments support the hot spot model, which has been already extensively discussed in the literature in the case of Kerr spacetime (Schnittman & Bertschinger 2004; Schnittman 2005, 2006; Broderick & Loeb 2005, 2006). For a 4 million Solar mass Kerr BH, the ISCO period ranges from about 30 minutes ($a/M = 0$) to 4 minutes ($a/M = 1$ and corotating orbit). In the case of SgrA*, the observed period of the flare quasi-periodic substructure ranges from 13 to about 30 minutes. NIR flares have been reported up to about 45 minutes [see Fig. 12 in Hamaus et al. (2009)]. This suggests that the orbital radius of the hot spot is not necessarily always at the ISCO, but it can vary and be at larger radii (Trippe et al. 2007). The shorter period ever measured is 13 ± 2 minutes, and it may be assumed either the ISCO period or, more conservatively, an upper bound for it. In the latter case, with a mass $M = 3.6 \cdot 10^6 M_\odot$ for SgrA*, one obtains $a/M \geq 0.70 \pm 0.11$ (Trippe et al. 2007)³.

The simplest hot spot model, which will be employed throughout this paper, is a single region of isotropic and monochromatic emission following a geodesic trajectory. Located on the equatorial plane, this hot spot is modeled as an optically thick emitting disk of finite radius. The local specific intensity of the radiation is chosen to have a Gaussian distribution in the local Cartesian space (Schnittman 2006)

$$I_{\text{em}}(\nu_{\text{em}}, x) \sim \delta(\nu_{\text{em}} - \nu_*) \exp \left[- \frac{|\tilde{\mathbf{x}} - \tilde{\mathbf{x}}_{\text{spot}}(t)|^2}{2R_{\text{spot}}^2} \right], \quad (1)$$

where ν_{em} is the photon frequency measured in the rest-frame of the emitter, while ν_* is the emission frequency of this monochromatic source. The spatial position 3-vector $\tilde{\mathbf{x}}$ is given in pseudo-Cartesian coordinates. Outside a distance of $4R_{\text{spot}}$ from the guiding geodesic trajectory $\tilde{\mathbf{x}}_{\text{spot}}$, there is no emission. Plausible values are $R_{\text{spot}} = 0.1 - 1.0M$, but it turns out that the light curves are not very sensitive to the exact spot size (see below and Fig. 4). More precisely, the light curve of the primary image is quite independent of it, while the effect of the spot size is more pronounced in the light curve of the secondary image, at least when the spot is orbiting very close to the compact object. Since we assume all points in the hot spot have the same 4-velocity as the geodesic guiding trajectory, one must be careful not to use a too large spot, or the point of emission $\tilde{\mathbf{x}}$ can be spatially far enough away from the center to make the results unphysical.

The calculation of the electromagnetic emission of a hot spot is, in many aspects, similar to the computation of the radiation emitted by a thin accretion disk (Li et al. 2005). The main difference is that the spectrum of the moving spot is time-dependent. First, we compute the trajectories of the photons backwards in time from the image plane of the distant observer to the orbital plane of the hot spot. The observer's sky is divided into a number of small elements and the ray-tracing procedure provides the observed time-dependent flux density from each element. In the special case of the Kerr background, one can exploit the properties of the Kerr solution and solve a simplified set of differential equations. Since in the next section we will consider non-Kerr spacetimes without these properties, we use the code described in Bambi (2012e), which solves the second-order photon geodesic equations by using the fourth-order

³ In Aschenbach et al. (2004) and Aschenbach (2006), the authors claimed the presence of a quasi-periodic substructure with a period of 5 minutes, which was interpreted as an indication that SgrA* is rotating very fast, with a/M close to 1. However, the analysis of the same data sets in Bélanger et al. (2006) did not find such a short period substructure.

Runge-Kutta-Nyström method (Lund et al. 2009). The initial conditions $(t_0, r_0, \theta_0, \phi_0)$ for the photon with Cartesian coordinates (X, Y) on the image plane of the distant observer and detection time t_{obs} are given by (Johannsen & Psaltis 2010)

$$t_0 = t_{\text{obs}}, \quad (2)$$

$$r_0 = \sqrt{X^2 + Y^2 + D^2}, \quad (3)$$

$$\theta_0 = \arccos \frac{Y \sin i + D \cos i}{r_0}, \quad (4)$$

$$\phi_0 = \arctan \frac{X}{D \sin i - Y \cos i}. \quad (5)$$

As the initial 3-momentum \mathbf{k}_0 must be perpendicular to the plane of the image of the observer, the initial conditions for the 4-momentum of the photon are

$$k_0^r = -\frac{D}{r_0} |\mathbf{k}_0|, \quad (6)$$

$$k_0^\theta = \frac{\cos i - (Y \sin i + D \sin i) \frac{D}{r_0^2}}{\sqrt{X^2 + (D \sin i - Y \cos i)^2}} |\mathbf{k}_0|, \quad (7)$$

$$k_0^\phi = \frac{X \sin i}{X^2 + (D \sin i - Y \cos i)^2} |\mathbf{k}_0|, \quad (8)$$

$$k_0^t = \sqrt{(k_0^r)^2 + r_0^2 (k_0^\theta)^2 + r_0^2 \sin^2 \theta_0 (k_0^\phi)^2}, \quad (9)$$

where D is the distance of the observer from the BH and i is the observer line of sight with respect to the BH spin. In the numerical calculations, the observer is located at the distance $D = 10^6 M$ (where M is the mass of the central compact object), which is far enough to assume that the background geometry is flat and therefore k_0^t can be inferred from the condition $g_{\mu\nu} k^\mu k^\nu = 0$ with the metric tensor of a flat spacetime.

The photon trajectory is numerically integrated backward in time from the image plane of the distant observer to the point of the photon emission on the orbital plane of the hot spot. We thus get the radial coordinate r_e at which the photon was emitted and the angle ξ between the wavevector of the photon and the normal of the orbital plane of the hot spot. The specific intensity of the radiation measured by the distant observer is given by

$$I_{\text{obs}}(\nu_{\text{obs}}, t_{\text{obs}}) = g^3 I_{\text{em}}(\nu_{\text{em}}, t_{\text{obs}}), \quad (10)$$

where g is the redshift factor

$$g = \frac{E_{\text{obs}}}{E_{\text{em}}} = \frac{\nu_{\text{obs}}}{\nu_{\text{em}}} = \frac{k_\alpha u_{\text{obs}}^\alpha}{k_\beta u_{\text{em}}^\beta}, \quad (11)$$

k_α is the 4-momentum of the photon, $u_{\text{obs}}^\alpha = (-1, 0, 0, 0)$ is the 4-velocity of the distant observer, and $u_{\text{em}}^\alpha = (u_{\text{em}}^t, 0, 0, \Omega u_{\text{em}}^t)$ is the 4-velocity of the emitter. Ω is the Keplerian angular frequency of a test-particle at the emission radius r_e . $I_{\text{obs}}(\nu_{\text{obs}})/\nu_{\text{obs}}^3 = I_{\text{em}}(\nu_{\text{em}})/\nu_{\text{em}}^3$ follows from the Liouville theorem. The hot spot emission is assumed to be monochromatic and isotropic, with a Gaussian intensity, as shown in Eq. (1). Using the normalization condition $g_{\mu\nu} u_{\text{em}}^\mu u_{\text{em}}^\nu = -1$, one finds

$$u_{\text{em}}^t = -\frac{1}{\sqrt{-g_{tt} - 2g_{t\phi}\Omega - g_{\phi\phi}\Omega^2}}, \quad (12)$$

and therefore,

$$g = \frac{\sqrt{-g_{tt} - 2g_{t\phi}\Omega - g_{\phi\phi}\Omega^2}}{1 + \lambda\Omega}, \quad (13)$$

where $\lambda = k_\phi/k_t$ is a constant of the motion along the photon path. Doppler boosting and gravitational redshift are entirely encoded in the redshift factor g . The effect of light bending is included by the raytracing calculation.

With the above machinery, we can compute the direct image of the hot spot at any observer's time t_{obs} . If the accretion disk around the BH is optically thick, as in the case of the one around stellar-mass BH candidates in binary systems in the X-ray band or of the accretion flow around SgrA* at mm wavelengths or above, light rays do not pass through the disk (which is supposed to be on the equatorial plane) and therefore we do not see multiple images. On the other hand, if the accretion flow is optically thin, as it is expected for SgrA* at shorter wavelengths (Falcke et al. 2000), light rays can pass through the disk and we can see multiple images of the hot spot, as a result of the gravitational lensing in the strong gravitational field around the object. Fig. 1 shows 5 instantaneous snapshots of a hot spot orbiting a Schwarzschild BH at the ISCO radius. These images are observed at time intervals $T/5$, where T is the orbital period of the hot spot. The hot spot has a radius $R_{\text{spot}} = 0.5 M$, it is moving anti-clockwise, and it is seen

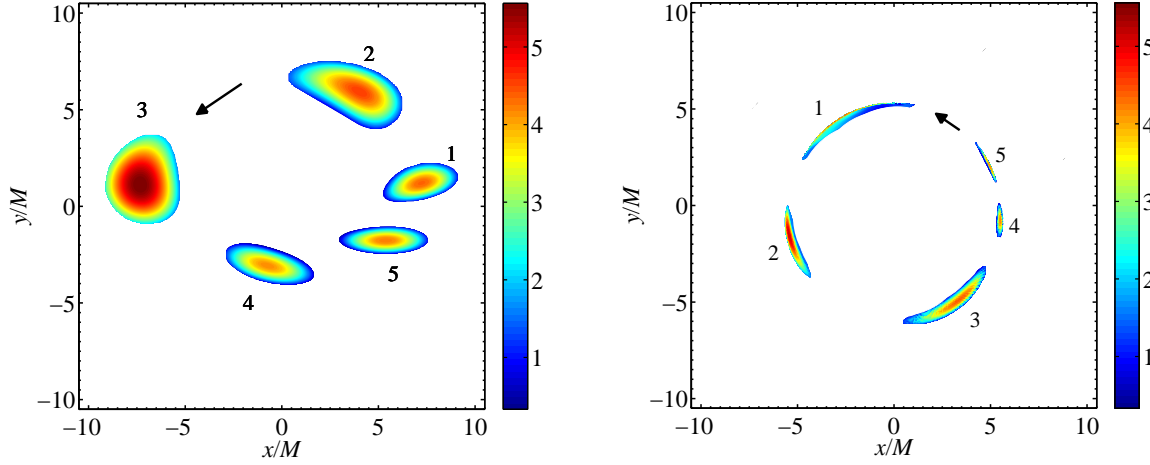


FIG. 1.— Left panel: specific intensity of primary images of a hot spot with a radius of $R_{\text{spot}} = 0.5 M$ orbiting a Schwarzschild BH at the ISCO. The observer's viewing angle is $i = 60^\circ$ and the time interval between two adjacent spot images is $T/5$, where T is the orbital period of the spot. Right panel: as in the left panel for the corresponding secondary images. Specific intensity in arbitrary units. See the text for more details.

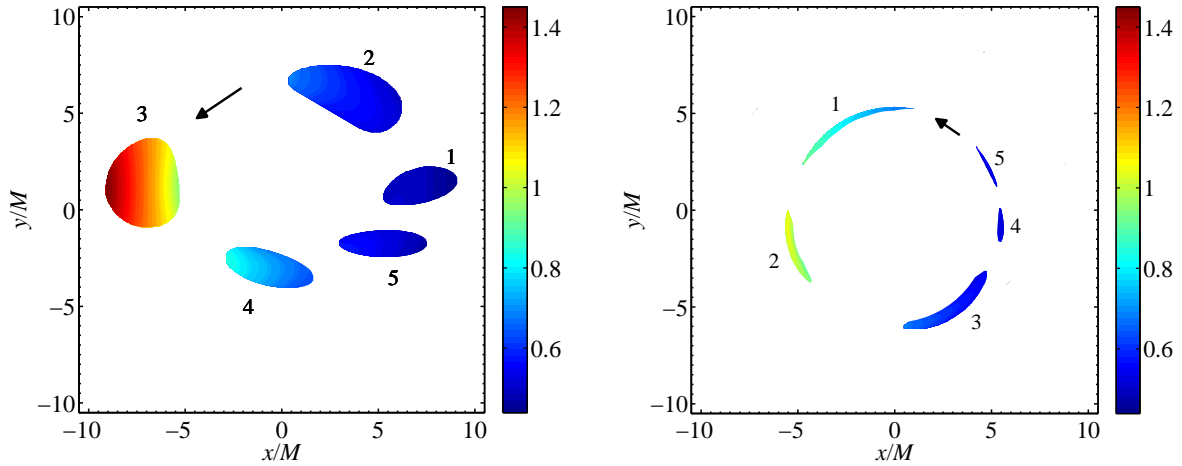


FIG. 2.— Left panel: redshift factor g of primary images of a hot spot with a radius of $R_{\text{spot}} = 0.5 M$ orbiting a Schwarzschild BH at the ISCO. The observer's viewing angle is $i = 60^\circ$ and the time interval between two adjacent spot images is $T/5$, where T is the orbital period of the spot. Right panel: as in the left panel for the corresponding secondary images. See the text for more details.

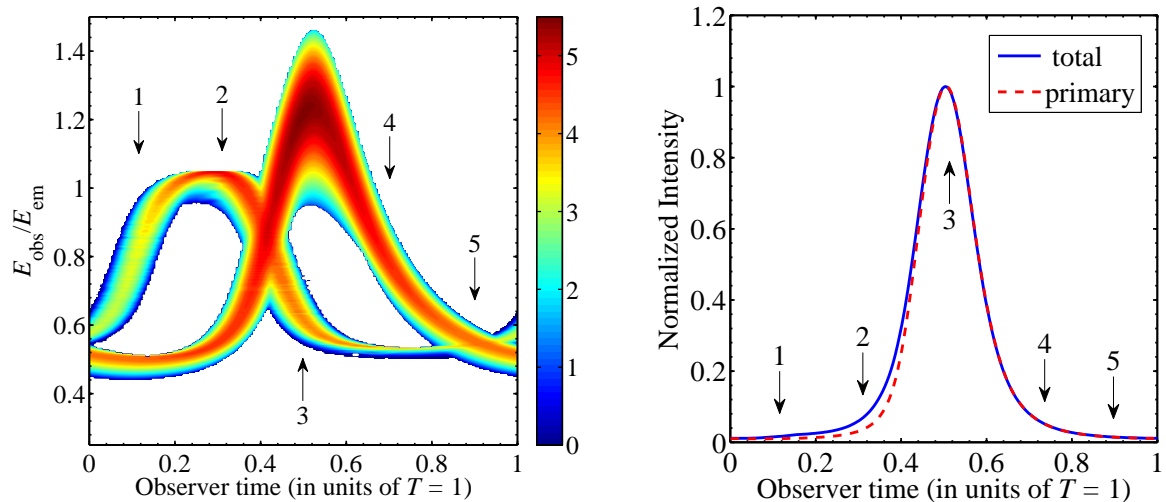


FIG. 3.— Left panel: spectrogram of a hot spot with a radius of $R_{\text{spot}} = 0.5 M$ orbiting a Schwarzschild BH at the ISCO. The observer's viewing angle is $i = 60^\circ$. Right panel: light curves of the same hot spot (blue solid line for the total light curve, red dashed line for the light curve of the primary image only). The five arrows refer to the five images shown in Figs. 1 and 2. See the text for more details.

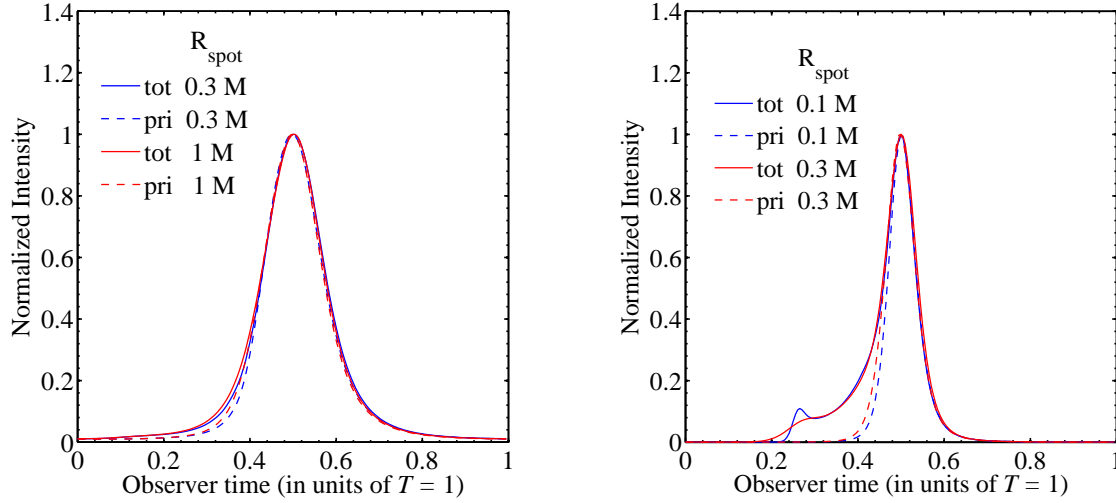


FIG. 4.— Left panel: light curves of hot spots with a radius of $R_{\text{spot}} = 0.3 M$ (blue/dark lines) and $1.0 M$ (red/light lines) orbiting a Schwarzschild BH at the ISCO. The observer’s viewing angle is $i = 60^\circ$. Solid lines for the total light curves, dashed lines for the primary image light curves. Right panel: as in the left panel for hot spots with a radius of $R_{\text{spot}} = 0.1 M$ (blue/dark lines) and $0.3 M$ (red/light lines) orbiting a Kerr BH with $a/M = 0.9$ at the ISCO. See the text for more details.

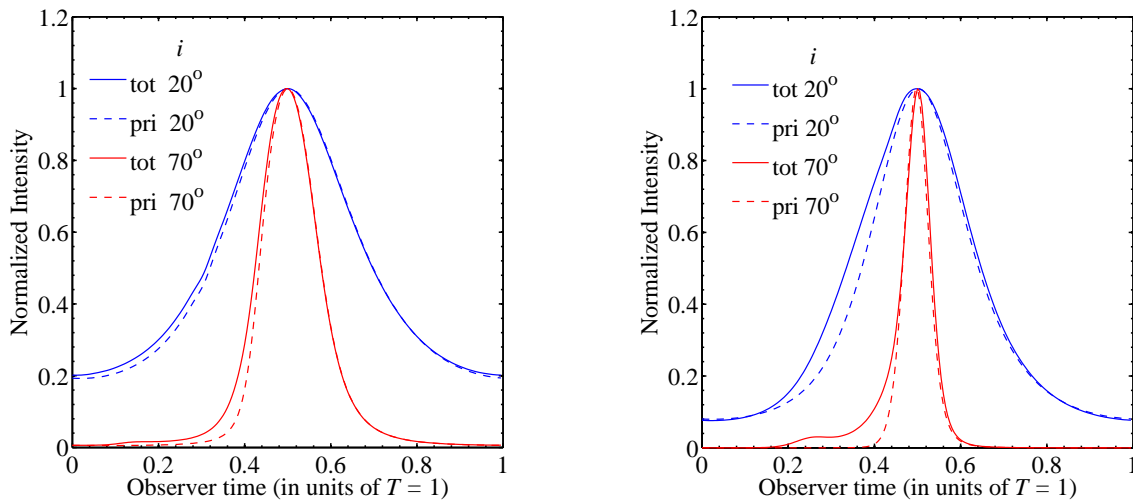


FIG. 5.— Left panel: light curves of a hot spot with a radius of $R_{\text{spot}} = 0.5 M$ orbiting a Schwarzschild BH at the ISCO. The observer’s viewing angle is $i = 20^\circ$ (blue/dark lines) and 70° (red/light lines). Solid lines for the total light curves, dashed lines for the primary image light curves. Right panel: as in the left panel for a hot spot with a radius of $R_{\text{spot}} = 0.3 M$ orbiting a Kerr BH with $a/M = 0.9$ at the ISCO. See the text for more details.

by an observer with viewing angle $i = 60^\circ$. The color of the images represents the relative specific intensity of the radiation (in arbitrary units). The left panel is for the primary images, the right panel for the secondary ones. The secondary images are clearly dimmer and around the apparent photon capture radius of the BH. The intensity of the center of the spot is always higher than the intensity of its edge because we are assuming the local specific intensity of Eq. (1). Fig. 2 shows the redshift factor g of the same images. With the GRAVITY instrument, one can expect to have NIR $10 \mu\text{as}$ astrometric measurements with a time resolution of about 1 minute (Hamaus et al. 2009), to be compared with the hot spot orbital period T of about 20 minutes. At radio and sub-mm wavelengths, integration times are significantly longer than in the NIR, and therefore radio and sub-mm facilities will not be able to detect these instantaneous images, but they will average them over the instrument time scale which is longer than the hot spot orbital period.

By integrating the observed specific intensity over the solid angle subtended by the image of the hot spot on the

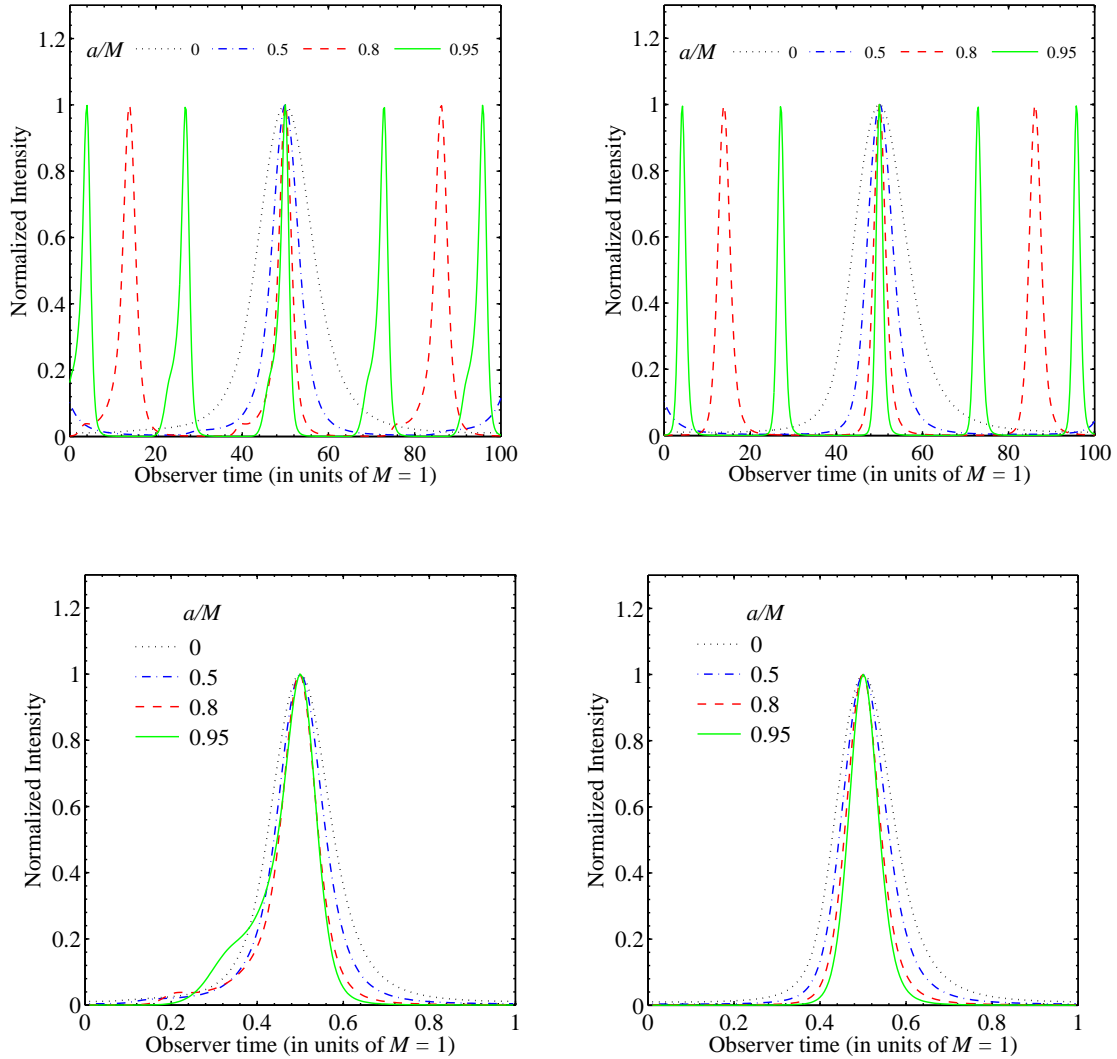


FIG. 6.— Top panels: light curves (left) and primary image light curves (right) of hot spots with a radius of $R_{\text{spot}} = 0.3 M$ orbiting Kerr BHs with spin $a/M = 0, 0.5, 0.8$ and 0.95 at the corresponding ISCO. The observer's viewing angle is $i = 60^\circ$. The frequency of the hot spot depends significantly on a/M , but an independent estimate of M is necessary. Bottom panels: as in the top panels, but with the observer's time in units $T = 1$, where T is the orbital period of the hot spot. See the text for more details.

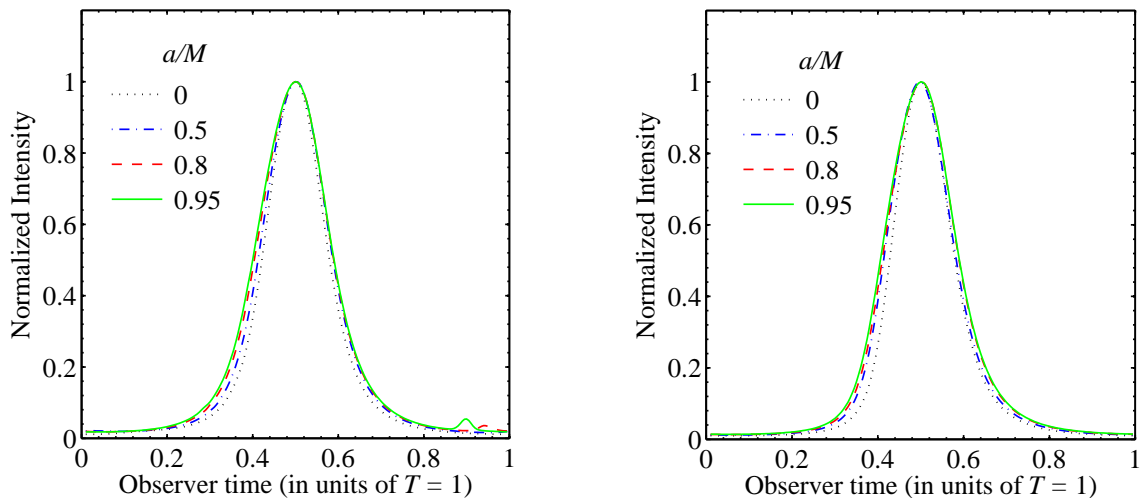


FIG. 7.— Left panel: light curves of hot spots with a radius of $R_{\text{spot}} = 0.3 M$ orbiting Kerr BHs with spin $a/M = 0, 0.5, 0.8$ and 0.95 . For $a/M = 0$, the hot spot is at the ISCO, while in the other cases the hot spot is at the radius with same Keplerian angular frequency as the one orbiting a Schwarzschild BH at the ISCO. The observer's viewing angle is $i = 60^\circ$. Right panel: as in the left panel for the primary images only. See the text for more details.

observer’s sky, we obtain the observed flux

$$F(\nu_{\text{obs}}, t_{\text{obs}}) = \int I_{\text{obs}}(\nu_{\text{obs}}, t_{\text{obs}}) d\Omega_{\text{obs}} = \int g^3 I_{\text{em}}(\nu_{\text{em}}, t_{\text{obs}}) d\Omega_{\text{obs}}. \quad (14)$$

The complete spectrogram of the hot spot of Figs. 1 and 2 is shown in the left panel of Fig. 3, where the numbers 1, ..., 5 refer to the time of the images with the same number in Figs. 1 and 2. For instance, the image numbered by 1 in Figs. 1 and 2 corresponds to the observer’s time $t/T = 0.1$ in Fig. 3. In this spectrogram, it is easy to identify the contribution coming from the primary image and the smaller one from the secondary image. If we integrate over the frequency range of the radiation, we get the observed luminosity, or light curve, of the hot spot

$$L(t_{\text{obs}}) = \int F(\nu_{\text{obs}}, t_{\text{obs}}) d\nu_{\text{obs}}. \quad (15)$$

The light curve of our hot spot is shown in the right panel of Fig. 3, where the blue/dark solid line is for the total light curve, while the red/light dashed line shows the one from the primary image only. In the present paper, we normalize the light curves by dividing the observed luminosity $L(t_{\text{obs}})$ by the corresponding maximum, since only the shape of the light curve can be used to determine the parameters of the model. Such a time-dependent emission signal can be added to a background intensity coming from the inner region of the steady state accretion disk. By definition, the hot spot will have a higher density and/or higher temperature and thus a higher emissivity than the background accretion disk, adding a small modulation to the total flux. For instance, in the case of stellar-mass BH candidates in X-ray binary systems, *RXTE* observations find the high-frequency QPO modulations to have typical amplitudes of 1% – 5% of the mean flux during the outburst (Remillard et al. 2002).

At this point, we can see the dependence of the light curve on the model parameters. The role of the size of the hot spot, its radius R_{spot} , is outlined in Fig. 4. The left panel shows the light curve of a hot spot orbiting a Schwarzschild BH at the ISCO; that is, at a radius $r = 6M$ in Boyer-Lindquist coordinates. The size of the spot is clearly not very important, both in the total light curve and in the primary image one. The right panel of Fig. 4 shows the light curve of a hot spot orbiting at the ISCO of a Kerr BH with $a/M = 0.9$. Now $r \approx 2.32M$. The effect of the spot size on the primary image light curve is larger than in the Schwarzschild case, but still moderate. The secondary image light curve is instead much more sensitive to the value of R_{spot} .

The effect of the inclination angle of the hot spot orbit with respect to the observer’s line of sight is shown in Fig. 5. The left panel is again for a hot spot orbiting at the ISCO radius around a Schwarzschild BH, while the right panel is for a Kerr BH with $a/M = 0.9$. As the inclination increases, the light curve goes from nearly sinusoidal to being sharply peaked by the special relativistic effect of light beaming. As already pointed out in Broderick & Loeb (2005), the value of the inclination angle determines the magnification of the hot spot and therefore it can be potentially estimated from the measurement of the latter (but in real data the situation seems to be more complicated).

The effect of the spin is shown in Fig. 6. If the hot spot is orbiting at the ISCO and we know the mass M of the BH, the spin determines the period of the light curve, which changes significantly from $a/M = 0$ to $a/M = 1$. In the top panels in Fig. 6, we chose a long enough time scale to include at least one period of each light curve, and we shifted one of the peaks of any light curve to the middle of the plot ($t = 50M$). At least in principle, even if we did not know the mass M , the spin could be inferred from the sole shape of the light curve, as shown in the bottom panels of Fig. 6. With real data, this seems however to be unlikely.

If the hot spot is orbiting at a radius larger than the one of the ISCO, the orbital period increases, as well as the period of the light curve. A natural question is if hot spots with the same orbital frequency but moving around Kerr BHs with different spin produce different light curves. The answer is partially positive: as shown in Fig. 7 for the total light curve (left panel) and the primary image light curve (right panel), but the difference is quite small. It is interesting to note that, for moderate and high spins, the total light curve has a small second peak due to the secondary image. Even if the hot spot is at a relatively large radius, the secondary image is sensitive to the BH spin. While the secondary maximum due to the secondary image is very low in the total light curve, and impossible to detect for present facilities like the ESO Very Large Telescope (VLT), it can leave specific signatures in the centroid track, which could be potentially observable for sufficiently bright spots and accurate astrometric measurements [see Section 4 of the present paper or Hamaus et al. (2009)].

3. HOT SPOTS ORBITING NON-KERR BLACK HOLES

As shown in the previous section, images and light curves of hot spot orbiting BHs are affected by a number of special and general relativistic effects, which produce specific signatures in the observed electromagnetic radiation. If the spacetime geometry around BH candidates is not described by the Kerr solution, the predicted images and light curves of hot spots are presumably different, and therefore their detection can potentially be used to test the Kerr nature of an astrophysical BH candidate. In this section, we show how possible deviations from the Kerr background can change the predictions of general relativity, while in the next section we will present a more quantitative analysis, paying some attention on the degeneracy/correlation between the estimate of the BH spin and the constraint on possible deviations from the Kerr metric.

In order to test the Kerr metric around BH candidates it is useful to adopt the following approach. We start considering a background metric more general than the Kerr solution and that includes the Kerr metric as a special case. Here the compact object is characterized by a mass M , a spin parameter a , and one (or even more) deformation parameter(s) which measures possible deviations from the Kerr geometry. When the deformation parameter vanishes, we exactly recover the Kerr metric. We can then compare the theoretical predictions obtained in this 3-parameter spacetime with observational data. If the latter demand a vanishing deformation parameter, the Kerr BH hypothesis is verified; if we find a non-vanishing deformation parameter, our data would suggest that the BH candidate is not of the Kerr type. In general, however, it is not easy to arrive at a clear conclusion, because most approaches are only sensitive to a particular observable quantity that may be produced by a Kerr BH with a specific spin a/M , as well as by many other non-Kerr BHs with different spin (Bambi 2013f). For instance, the continuum-fitting method actually measures something like the radiative efficiency in the Novikov-Thorne model, $\eta_{\text{NT}} = 1 - E_{\text{ISCO}}$, where E_{ISCO} is the specific energy of a test particle at the ISCO. In the Kerr background, there is a one-to-one correspondence between η_{NT} and a/M , and therefore this technique can be used to estimate the spin parameter of the BH. However, if we also have a deformation parameter, η_{NT} depends on both the spin and the deformation parameter. If we fix the deformation parameter, the same value of η_{NT} is found for a particular value of the spin, at least if the deformation parameter is not too large. Such a degeneracy/strong correlation between the spin and the deformation parameter can be fixed either by combining two measurements sensitive to very different properties of the background metric (Bambi 2012b,c,d), or by an observable quantity that is not sensitive to only one number.

As non-Kerr background, here we consider the Johannsen-Psaltis metric (Johannsen & Psaltis 2011b). While the latter is not a solution of any known gravity theory, and for some values of the background parameters it presents several pathological features, it is a simple metric that parametrizes possible deviations from the Kerr geometry. In most cases, observations can only check if the gravitational force around a BH with spin parameter a/M is stronger or weaker than the one around a Kerr BH with the same spin, without being able to probe the unphysical region with pathological features. In Boyer-Lindquist coordinates, the metric is given by the line element (Johannsen & Psaltis 2011b)

$$ds^2 = - \left(1 - \frac{2Mr}{\Sigma}\right) (1+h) dt^2 + \frac{\Sigma(1+h)}{\Delta + a^2 h \sin^2 \theta} dr^2 + \Sigma d\theta^2 - \frac{4aMr \sin^2 \theta}{\Sigma} (1+h) dt d\phi \\ + \left[\sin^2 \theta \left(r^2 + a^2 + \frac{2a^2 Mr \sin^2 \theta}{\Sigma} \right) + \frac{a^2 (\Sigma + 2Mr) \sin^4 \theta}{\Sigma} h \right] d\phi^2, \quad (16)$$

where $\Sigma = r^2 + a^2 \cos^2 \theta$, $\Delta = r^2 - 2Mr + a^2$, and

$$h = \sum_{k=0}^{\infty} \left(\epsilon_{2k} + \frac{Mr}{\Sigma} \epsilon_{2k+1} \right) \left(\frac{M^2}{\Sigma} \right)^k. \quad (17)$$

This metric has an infinite number of deformation parameters ϵ_i , and the Kerr solution is recovered when all the deformation parameters are set to zero. However, in order to reproduce the correct Newtonian limit, we have to impose $\epsilon_0 = \epsilon_1 = 0$, while ϵ_2 is strongly constrained by Solar System experiments (Johannsen & Psaltis 2011b). In this paper, we will only examine the simplest cases where $\epsilon_3 \neq 0$, while all the other deformation parameters vanish. The choice of another deformation parameter would not qualitatively change our results and conclusions. Negative ϵ_i s make always the BH more oblate and therefore the gravitational force on the equatorial plane is stronger, with the result that the ISCO radius is larger and the ISCO orbital period longer. Positive ϵ_i s have the opposite effect, but the ISCO radius and the ISCO period first decrease and then increase as ϵ_i increases. The qualitative effect of any deformation parameter is the same, see e.g. Bambi (2012a). The presence of more than one non-vanishing deformation parameter makes the discussion more complicated, but it does not introduce any new feature and for this reason we can restrict the attention to ϵ_3 .

Figs. 8 and 9 show the effect of the deformation parameter ϵ_3 on the (total) light curve of a hot spot. In Fig. 8, we assume that the hot spot is at the ISCO. Here, the major effect is the variation of the ISCO radius, which implies a different hot spot orbital period (left panel). However, an independent estimate of the mass M , which sets the characteristic scale of the system, must be known. If we consider the case in which we do not know at all M (this is not the case of SgrA*, even if at present the uncertainty on its measurement is quite large, around 10%), we can compare light curves over an orbital period, as shown in the right panel in Fig. 8. A different deformation parameter still produces a light curve with a slightly different shape. In the end, if the hot spot is at the ISCO, the deformation parameter plays more or less the same role as the spin a/M , discussed in Fig. 6.

The case of hot spots orbiting non-Kerr BHs at radii with the same orbital frequency is shown in Fig. 9. As in the Kerr background in Fig. 7, light curves with the same period have a slightly different shape due to the different background metric. The left panel in Fig. 9 shows the total light curve of hot spots orbiting around non-Kerr BHs with $a/M = 0.5$ for different values of the deformation parameter ϵ_3 . The right panel compares instead the light curve associated to hot spots orbiting non-Kerr BHs with $\epsilon_3 = 3$ and different values of the spin a/M . In conclusion, it seems that the spin and possible deviations from the Kerr solution affect the light curve of hot spots in a quite similar way. In the next section, we will be more quantitative, and we will see how the spin and the deformation parameter ϵ_3 are correlated, as well as if and how it is possible to get an independent estimate of them.

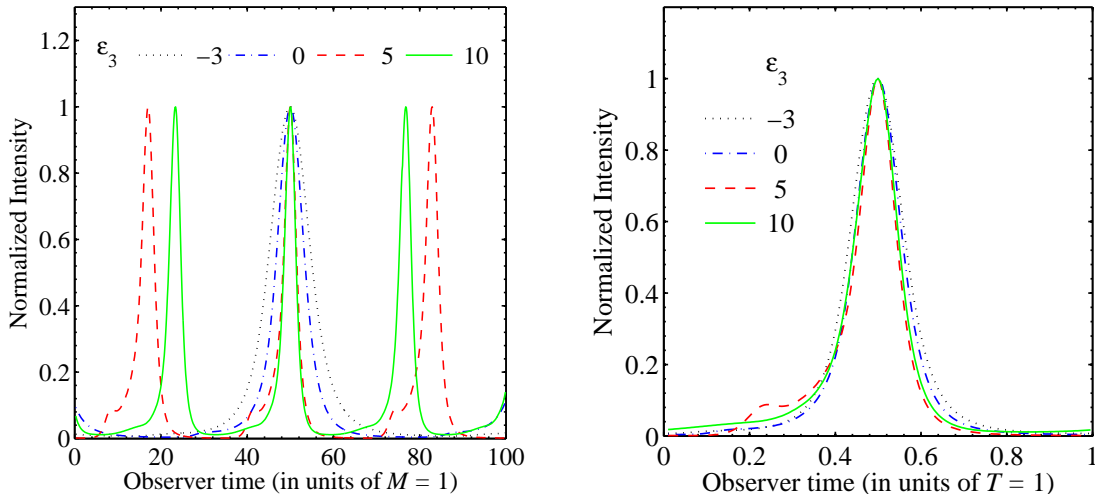


FIG. 8.— Left panel: light curves of hot spots with a radius of $R_{\text{spot}} = 0.3M$ orbiting Johannsen-Psaltis BHs with $a/M = 0.5$ and $\epsilon_3 = -3, 0, 5, 10$ at the ISCO. The observer’s viewing angle is $i = 60^\circ$. Right panel: as in the left panel, but with the observer’s time in units $T = 1$, where T is the orbital period of the hot spot. See the text for more details.

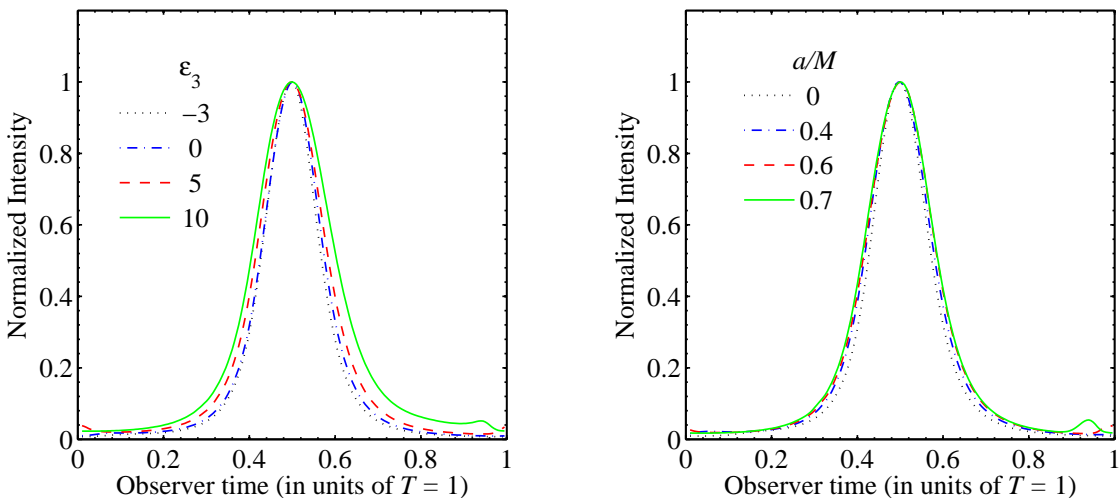


FIG. 9.— Left panel: light curves of hot spots with a radius of $R_{\text{spot}} = 0.3M$ orbiting Johannsen-Psaltis BHs with $a/M = 0.5$ and $\epsilon_3 = -3, 0, 5, 10$. The hot spot is at the radius with the same angular frequency as the one at the ISCO of the BH with $\epsilon_3 = -3$. The observer’s viewing angle is $i = 60^\circ$. Right panel: light curves of hot spots with a radius of $R_{\text{spot}} = 0.3M$ orbiting Johannsen-Psaltis BHs with $a/M = 0.0, 0.4, 0.6, 0.7$ and $\epsilon_3 = 3$. The hot spot is at the radius with the same angular frequency as the one at the ISCO of the BH with $a/M = 0$. See the text for more details.

4. DISCUSSION

The light curve of a hot spot is characterized by a time scale, set by the hot spot orbital period, and by a magnification, mainly determined by the orbital inclination with respect to the line of sight of the distant observer. The spin and possible deviations from the Kerr solution set the ISCO radius and therefore the ISCO frequency. The exact shape of the light curve also depends on the background metric, but the effects are smaller. In order to be more quantitative and figure out the information carried by the light curve, we can compare light curves produced in Kerr and non-Kerr spacetimes. We define the reduced χ^2 as

$$\chi_{\text{red}}^2(a/M, \epsilon_3) = \frac{\chi^2}{n-2} = \frac{1}{n-2} \sum_{i=1}^n \frac{[L_i^{\text{Sim}}(\bar{a}/M, \bar{\epsilon}_3) - L_i^{\text{Th}}(a/M, \epsilon_3)]^2}{\sigma^2}, \quad (18)$$

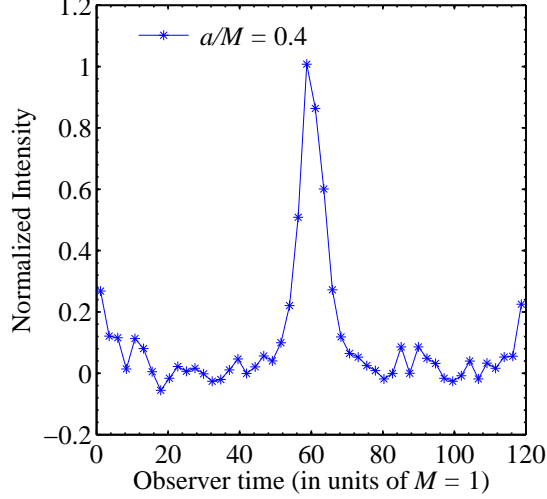


FIG. 10.— Simulated total light curve of a hot spot orbiting the ISCO of a Kerr BH with $\tilde{a}/M = 0.4$.

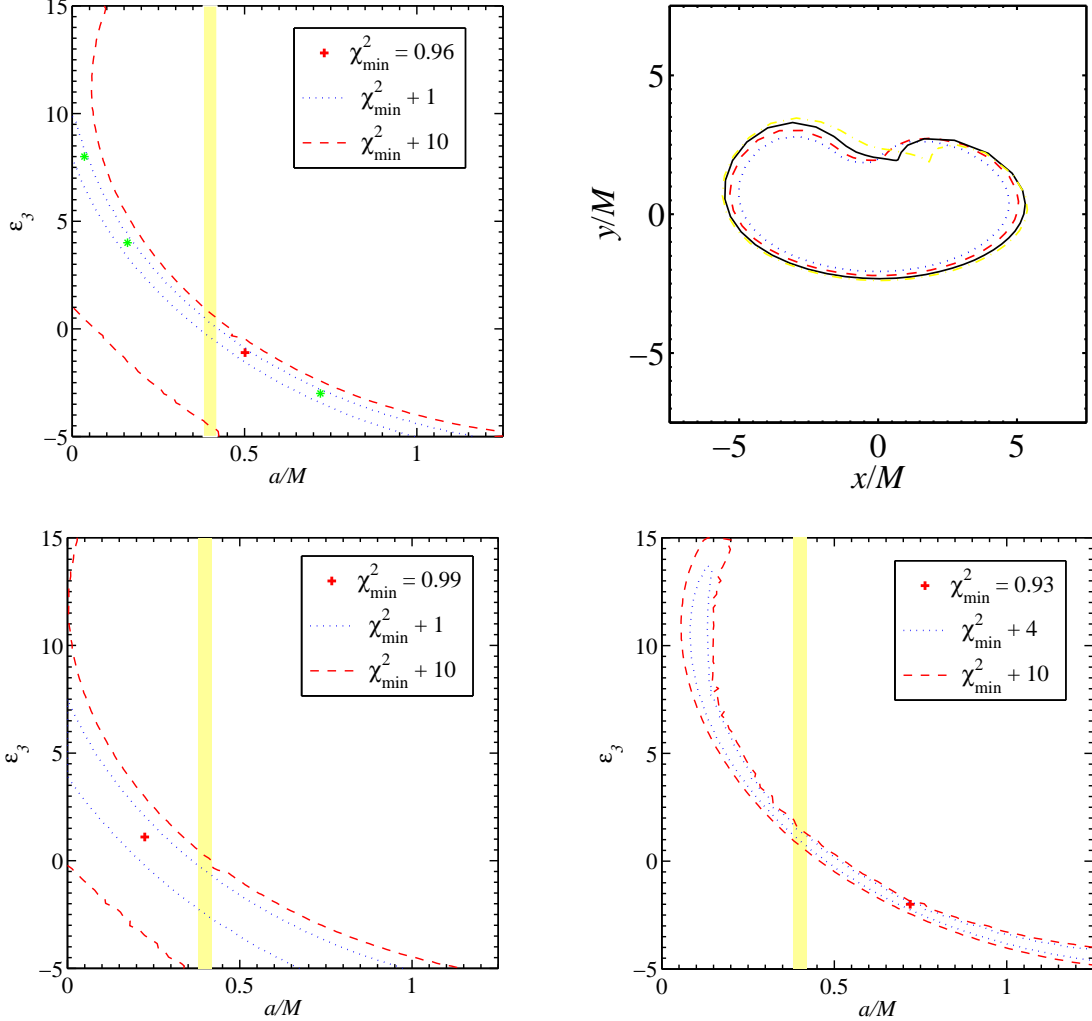


FIG. 11.— Top left panel: χ_{red}^2 from the comparison of the simulated total light curve of a hot spot orbiting the ISCO of a Kerr BH with $\tilde{a}/M = 0.4$ (shown in Fig. 10) and of the theoretical light curves expected from hot spots orbiting the ISCO of Johannsen-Psaltis BHs. Light curves from hot spots in spacetimes with the same ISCO frequency are eventually indistinguishable. The hot spot size is $R_{\text{spot}} = 0.3 M$ and the observer's viewing angle is $i = 60^\circ$. The yellow area corresponds to a possible BH spin measurement $a/M = 0.40 \pm 0.01$ from a radio pulsar in a compact orbit in the case in which SgrA* has $a/M = 0.4$ (such a measurement would be independent of ϵ_3). Top right panel: centroid tracks of hot spots orbiting the ISCO of BHs with $a/M = 0.04$ and $\epsilon_3 = 8$ (blue dotted curve), $a/M = 0.16$ and $\epsilon_3 = 4$ (red dashed curve), $a/M = 0.4$ and $\epsilon_3 = 0$ (black solid curve), and $a/M = 0.72$ and $\epsilon_3 = -3$ (yellow dashed-dotted curve). These four spacetimes correspond to the one of the simulated light curve and to the ones associated to the three green stars in the left panel. Bottom panels: as in the top left panel in the case of simulated light curves in a Kerr spacetime with $\tilde{a}/M = 0.3$ (right panel) and 0.5 (left panel). See the text for more details.

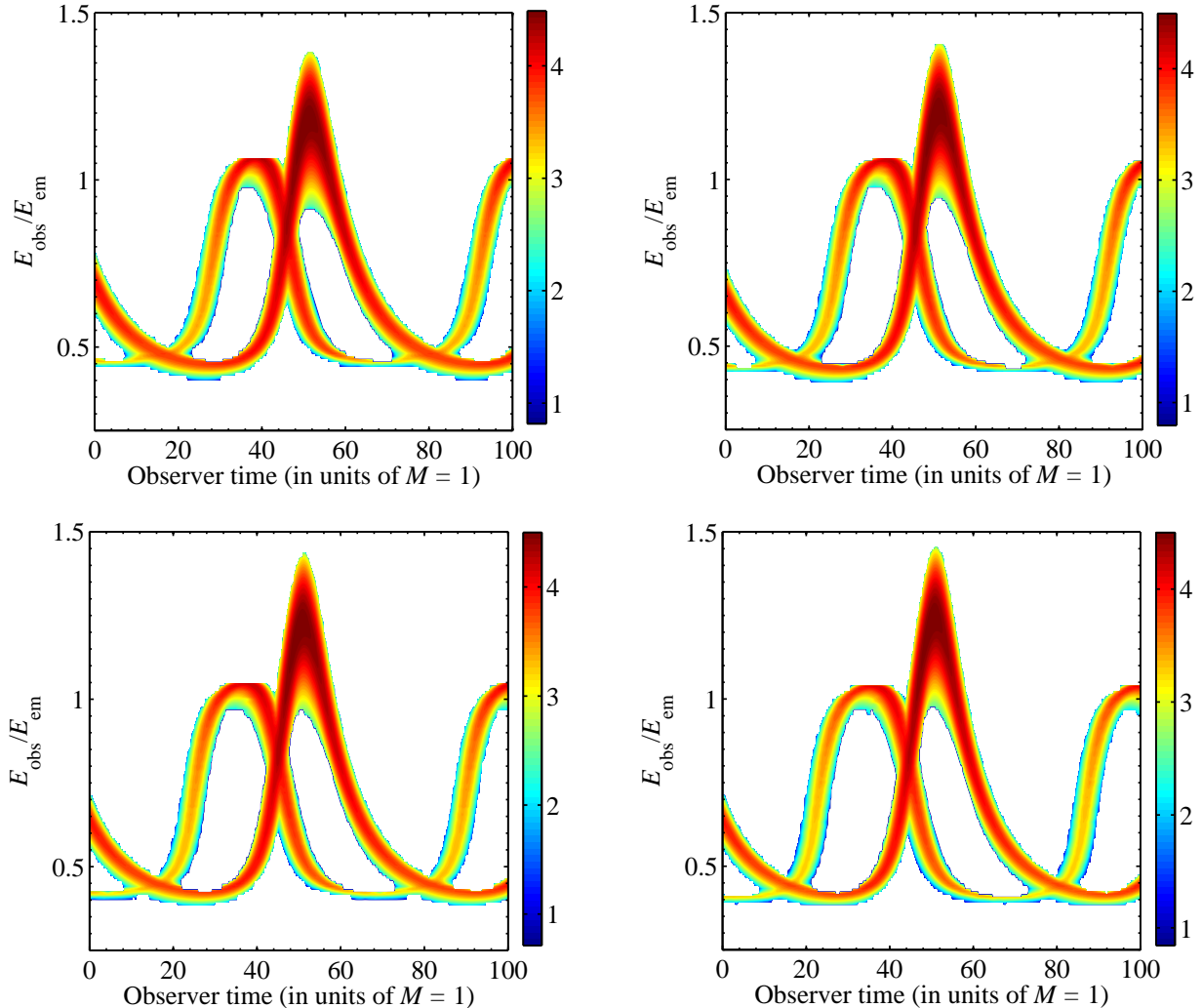


FIG. 12.— Hot spot spectrograms for $a/M = 0.04$ and $\epsilon_3 = 8$ (top left panel), $a/M = 0.16$ and $\epsilon_3 = 4$ (top right panel), $a/M = 0.4$ and $\epsilon_3 = 8$ (bottom left panel), $a/M = 0.72$ and $\epsilon_3 = -3$ (bottom right panel). These spacetimes correspond to the ones marked by a green star in the top left panel in Fig. 11 and to the one of the simulated light curve. See the text for more details.

where the summation is performed over $n = 50$ sampling times t_i . L_i^{Sim} is a simulated (i.e. noisy) normalized light curve calculated in the spacetime with spin \tilde{a}/M and deformation parameter $\tilde{\epsilon}_3$. Such a light curve is generated by assuming a Gaussian noise of 10%. L_i^{Th} is instead the theoretical prediction for a light curve in a spacetime with spin a/M and deformation parameter ϵ_3 . The error σ is assumed to be 4% of the value of the peak of L_i^{Sim} and it does not depend on L_i^{Sim} because the amplitude of the quasi-periodic modulation is much smaller than the mean flux of the flare. Such a value roughly corresponds to the error of current observations with the ESO-VLT facility; see e.g. the figures in Trippe et al. (2007) or in Hamaus et al. (2009). In the case of higher or lower values of σ , one has just to rescale χ_{red}^2 , without altering its shape.

The mass of SgrA* is estimated to be around 4 million Solar masses, with an uncertainty of about 10%. Even assuming the Kerr metric, both the spin and the inclination angle are not really constrained to date, in the sense that different authors give quite different results. Cosmological evolution arguments suggest that, generally speaking, supermassive BHs are today not rotating rapidly (Li et al. 2012). However, the case of SgrA* is more controversial and actually many GRMHD simulations give high spin best fits, see e.g. Drapeau et al. (2013). The inclination of SgrA* cannot be straightforwardly derived from the magnification of the hot spot, as the observed data show a complicated signal, which is the superposition of a plausible sinusoidal component (that may be a hot spot) and a gaussian envelope. In what follows, we consider a specific case as an example to illustrate the main purpose of the present work, which is how the observation of a hot spot can be used to test the Kerr nature of SgrA*, without having in mind specific values of the BH parameters.

Let us first assume that SgrA* is a Kerr BH with $\tilde{a}/M = 0.4$ and that we observe a hot spot orbiting at the ISCO radius. The simulated light curve is shown in Fig. 10. For the sake of simplicity, we fix the observer's inclination angle $i = 60^\circ$ and the hot spot size $R_{\text{spot}} = 0.3 M$. The reduced χ^2 is reported in the top left panel of Fig. 11, which shows

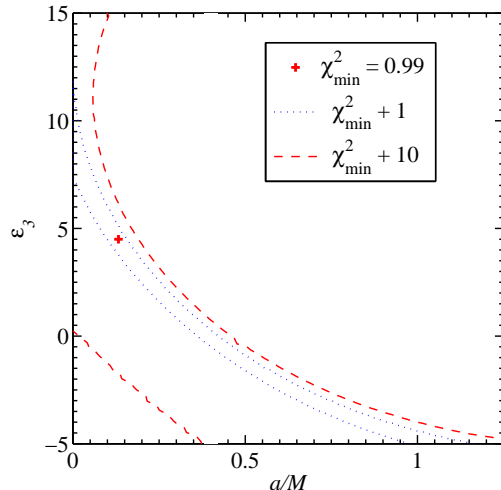


FIG. 13.— As in the top left panel of Fig. 11 in the case of a simulated light curve in Johannsen-Psaltis spacetime with $\tilde{a}/M = 0.16$ and $\tilde{\epsilon}_3 = 4$.

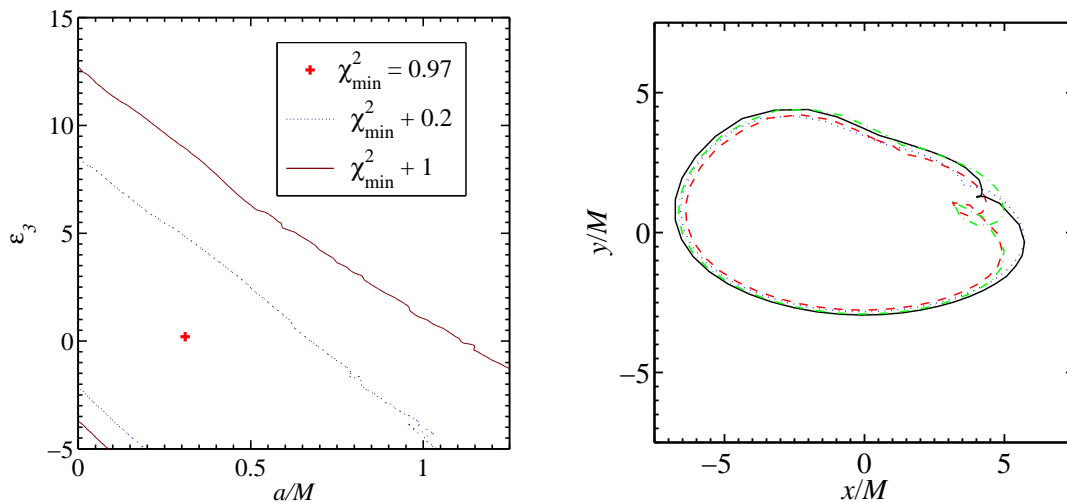


FIG. 14.— Left panel: χ^2_{red} from the comparison of the simulated total light curve of a hot spot orbiting a Kerr BH with $\tilde{a}/M = 0.4$ at the radius whose orbital frequency is the same as the one of the ISCO of a Schwarzschild BH and the theoretical light curves expected from hot spots orbiting Johannsen-Psaltis BHs at a radius with the same orbital frequency. The hot spot size is $R_{\text{spot}} = 0.3M$ and the observer's viewing angle is $i = 60^\circ$. Right panel: centroid tracks of hot spots orbiting around BHs with $a/M = 0.4$ and $\epsilon_3 = 0$ (black solid curve), $a/M = 0.7$ and $\epsilon_3 = 0$ (green dashed-dotted curve), $a/M = 0.4$ and $\epsilon_3 = 5$ (red dashed curve), $a/M = 0.1$ and $\epsilon_3 = 5$ (blue dotted curve) at a radius with the same orbital frequency as the one of the ISCO of a Schwarzschild BH. See the text for more details.

that the hot spot light curve can only select those spacetimes with the same ISCO frequencies, while the differences due to the background metric are too small to provide any useful information. In such a situation, one would like thus to figure out if additional observations can break the correlation between spin and possible deviations from the Kerr geometry. The VLTI instrument GRAVITY will be able to image hot spot orbiting around SgrA* with an angular resolution of about $10 \mu\text{as}$ (which correspond to about $2M$) and a time resolution of about 1 minute. The three green stars in the top left panel of Fig. 11 correspond to the minima of the reduced χ^2 for $\epsilon_3 = 8, 4, -3$. The centroid tracks in these spacetimes and the one in a Kerr background corresponding to the simulated light curve are reported in the top right panel of Fig. 11 [the centroid at any time is calculated following Hamaus et al. (2009)]. The ISCO frequency of these backgrounds is essentially the same and the four light curves are practically indistinguishable. The shape of the centroid tracks is different. The origin of this difference is the contribution of the secondary image, whose peak phase shift with respect to the peak of the primary image changes a little bit with the background metric (see Fig. 12). Considering that the differences among these centroid tracks is not larger than M and that we are assuming a quite simple hot spot model (the emission will not be really monochromatic and the hot spot will likely be stretched due to shearing close to the BH), the GRAVITY instrument will be unable to distinguish these spacetimes. The effect of the BH mass uncertainty is shown in the bottom panels of Fig. 11. If the BH mass is larger (smaller) than 10%, the ISCO

frequency found for a Kerr BH with $\tilde{a}/M = 0.4$ corresponds instead to a Kerr BH with $\tilde{a}/M \approx 0.5$ (0.3). The bottom panels in Fig. 11 show the reduced χ^2 for a simulated light curve calculated in a Kerr background with $\tilde{a}/M = 0.3$ (left panel) and 0.5 (right panel).

A more attracting possibility to test the spacetime geometry around SgrA* is to combine the hot spot information with the measurements of the BH mass and spin that could be obtained from accurate radio observations of a radio pulsar in a compact orbit around SgrA*. At present, no similar pulsar is known, but there are a lot of efforts to find pulsars around the supermassive BH candidate at the Center of our Galaxy and their discovery is probably only an issue of time. A pulsar with an orbital period of a few months would provide very accurate measurements of the BH mass and spin, as discussed in Liu et al. (2012). The key-point here is that the pulsar is in the weak gravitational field of SgrA*, where the mass is the monopole term of the gravitational field, the spin is the dipole term, and deviations from the Kerr solutions would appear at higher orders. The pulsar measurement therefore provides the actual spin, independently if it is orbiting around a Kerr or non-Kerr BH. The yellow vertical line in Fig. 11 is the possible spin measurement $a/M = 0.40 \pm 0.01$ from a similar radio pulsar. The combination of these measurement with the ISCO frequency of the hot spot would result in a quite small allowed area; that is, possible deviations from the Kerr solutions can be strongly constrained. Here one may argue that the sole observation of the radio pulsar may test the quadrupole moment of SgrA* and therefore check if it is consistent with the predictions of the Kerr metric (Liu et al. 2012). While that is definitively true, there are two significant advantages with the use of the hot spot information. First, the pulsar may only test the quadrupole moment of SgrA*, while this object may have the same quadrupole moment as a Kerr BH and have deviations starting from higher order moments. The hot spot near the ISCO would be sensitive to these higher order deviations. Second, the pulsar can test the quadrupole moment of SgrA* only in the case it is a very fast-rotating BH (Liu et al. 2012). The hot spot does not require it.

Let us now consider the possibility that SgrA* is a Johannsen-Psaltis with $\tilde{a}/M = 0.16$ and $\tilde{\epsilon}_3 = 4$. The reduced χ^2 is shown in Fig. 13. As it could be expected, the hot spot light curve can only select the spacetime with the same ISCO frequency, and the reduced χ^2 in Fig. 13 has exactly the same structure as the ones in Fig. 11.

We note that our hot spot model relies on two important assumptions. First, the hot spot is supposed to orbit at the ISCO radius. Assuming that the hot spot model is correct, present data show that the timescale of the substructure of the flares ranges from 13 to 30 minutes. That would suggest that the hot spot is not necessary at the ISCO radius, but the clumps of matter can form at different radii before being destroyed after a few orbits (Trippe et al. 2007). We may argue that one could consider the shortest timescale never observed as a proxy of the ISCO period, but this is still a strong assumption. To be more fair, even the shortest timescale would provide an upper bound to the ISCO period. One can relax the assumption that the hot spot is at the ISCO and consider the more general case with the hot spot radius as a free parameter, but in this case it is quite difficult to put constraints on the model. The second important assumption is the monochromatic emission of the spot. That does not affect the hot spot frequency, but it plays a major role in the calculation of the hot spot image and therefore in the prediction of the centroid track [it significantly changes the redshift factor, see e.g. Eq. (6) in Hamaus et al. (2009)]. Here we have just considered the simplest case and if one really wants to use the centroid track to constrain the geometry around SgrA* a more detailed analysis with more realistic emission models would be necessary.

If we relax the assumption that the hot spot is orbiting at the ISCO radius, the estimate of a/M and ϵ_3 is more challenging. The reduced χ^2 of this case is shown in the left panel of Fig. 14. The simulated light curve is calculated in a Kerr spacetime with $\tilde{a}/M = 0.4$. The hot spot orbital frequency is the same as the one at the ISCO of a Schwarzschild BH. As in the previous examples, we introduced a Gaussian noise of 10%. The theoretical light curves are computed for any spacetime at the radius with an orbital frequency equal to the one of the simulated light curves. The final result is that the hot spot cannot put any constraint on the spin-deformation parameters plane. In the end, it is true that one cannot really extract much more information than the orbital frequency. In Fig. 14, we also report the curve $\chi^2_{\min} + 0.2$ just to better show the shape of the reduced χ^2 . If we consider the centroid tracks of different spacetimes, it turns out that the shape of the track is different. This is reported in the right panel of Fig. 14, which shows the cases $a/M = 0.4$ and $\epsilon_3 = 0$ (black solid curve), $a/M = 0.7$ and $\epsilon_3 = 0$ (green dashed-dotted curve), $a/M = 0.4$ and $\epsilon_3 = 5$ (red dashed curve), $a/M = 0.1$ and $\epsilon_3 = 5$ (blue dotted curve). However, as in the previous case of a hot spot at the ISCO radius, GRAVITY will not be able to distinguish these metrics.

5. SUMMARY AND CONCLUSIONS

SgrA*, the supermassive BH candidate at the Center of our Galaxy, shows X-ray and NIR flares of 1-3 hours at a rate of a few per day. Every flare has a quasi-periodic substructure with a time scale of about 20 minutes. The hot spot model explains such a substructure with the presence of a compact emitting region orbiting near the ISCO of SgrA*. This scenario can be hopefully confirmed by the near future VLTI instrument GRAVITY, which has the capability to image the hot spot and observe its motion. The possibility of observing a bright compact source near the ISCO of SgrA* can be used to probe the spacetime geometry around this object and verify if it is a Kerr BH, as expected in general relativity.

In the present paper, we have extended previous results found in the Kerr background to the case of non-Kerr metrics, to figure out how the observation of a hot spot near the ISCO radius can test the Kerr nature of SgrA*. As in the case of other techniques, the main problem is the strong correlation between effects due to the spin and the

ones coming from possible deviations from the Kerr solution. Since the BH mass is measured by dynamical methods, by studying the orbital motion of individual stars at relatively large distances from the compact object and in the framework of Newtonian gravity, the spin is the only background parameter if we assume that SgrA* is a Kerr BH. Any observable quantity determined by the geometry of the spacetime can be used to infer the value of the spin. If we want to test the Kerr metric of SgrA*, in addition to the spin we have a deformation parameter, which is used to quantify possible deviations from the Kerr solution. Now the observable quantity depends on two parameters and it is not easy to get an independent estimate of both.

If we assume that the quasi-periodic substructure with the shortest timescale is produced by hot spots at the ISCO of SgrA*, the hot spot light curve provides the ISCO frequency. In the case of a non-Kerr background with one deformation parameter, one finds an allowed region on the spin-deformation parameter plane. Light curves in different metric are not exactly the same, but the difference is so small that it cannot be identified with current and near future facilities, so eventually only the period of the hot spot matters. For this reason, if we want to test the Kerr nature of SgrA* we need additional measurements. GRAVITY will be able to observe the orbital motion of a hot spot orbiting near the ISCO of the supermassive BH candidate at the Center of the Galaxy with an angular resolution of order $10 \mu\text{as}$ and a time resolution of about 1 minute. If the hot spot model is correct, the centroid track depends on the background metric and BH spacetimes with the same ISCO frequency have centroid tracks with different shape, which means that the simultaneous measurement of the orbital frequency and of the image of the hot spot can potentially break the degeneracy between spin and possible deviations from the Kerr geometry. However, that is out of reach for GRAVITY. A more appealing possibility is represented by the discovery of a radio pulsar in a compact orbit (orbital period of a few months) around SgrA*. In such a case, accurate radio observations would be able to get precise measurements of the BH mass and spin in the weak field regime, independently of possible deviations from the Kerr solution. The combination of these measurements with the hot spot constraint would provide a stringent test of the Kerr BH hypothesis.

We thank Rohta Takahashi for useful discussions and suggestions. This work was supported by the NSFC grant No. 11305038, the Shanghai Municipal Education Commission grant for Innovative Programs No. 14ZZ001, the Thousand Young Talents Program, and Fudan University.

REFERENCES

- Abdujabbarov, A., Atamurotov, F., Kucukakca, Y., Ahmedov, B., & Camci, U. 2013, *Ap&SS*, 344, 429
- Abramowicz, M. A., Kluźniak, W., & Lasota, J.-P. 2002, *A&A*, 396, L31
- Amarilla, L., & Eiroa, E. F. 2012, *Phys. Rev. D*, 85, 064019
- Amarilla, L., & Eiroa, E. F. 2013, *Phys. Rev. D*, 87, 044057
- Amarilla, L., Eiroa, E. F., & Giribet, G. 2010, *Phys. Rev. D*, 81, 124045
- Aschenbach, B. 2006, *Chinese Journal of Astronomy and Astrophysics Supplement*, 6, 010000
- Aschenbach, B., Grosso, N., Porquet, D., & Predehl, P. 2004, *A&A*, 417, 71
- Bambi, C. 2011a, *Physics Letters B*, 705, 5
- Bambi, C. 2011b, *Modern Physics Letters A*, 26, 2453
- Bambi, C. 2012a, *Phys. Rev. D*, 85, 043001
- Bambi, C. 2012b, *Phys. Rev. D*, 85, 043002
- Bambi, C. 2012c, *Phys. Rev. D*, 86, 123013
- Bambi, C. 2012d, *J. Cosmol. Astropart. Phys.*, 9, 14
- Bambi, C. 2012e, *ApJ*, 761, 174
- Bambi, C. 2013a, *Phys. Rev. D*, 87, 023007
- Bambi, C. 2013b, *The Astronomical Review*, 8, 4
- Bambi, C. 2013c, *Phys. Rev. D*, 87, 084039
- Bambi, C. 2013d, *Phys. Rev. D*, 87, 107501
- Bambi, C. 2013e, *Scientific World J.*, 2013, 204315
- Bambi, C. 2013f, *J. Cosmol. Astropart. Phys.*, 8, 55
- Bambi, C. 2013g, *arXiv:1312.2228*
- Bambi, C. 2014a, *Physics Letters B*, 730, 59
- Bambi, C. 2014b, *J. Cosmol. Astropart. Phys.*, 3, 34
- Bambi, C., & Barausse, E. 2011, *ApJ*, 731, 121
- Bambi, C., Caravelli, F., & Modesto, L. 2012, *Physics Letters B*, 711, 10
- Bambi, C., & Freese, K. 2009, *Phys. Rev. D*, 79, 043002
- Bambi, C., Freese, K., & Takahashi, R. 2010, *Is the Carter-Israel conjecture correct?*, in *Windows on the Universe*, edited by L. Celnikier et al. (The Gioi Publishers, Ha Noi, Vietnam), pp. 575-578
- Bambi, C., & Malafarina, D. 2013, *Phys. Rev. D*, 88, 064022
- Bambi, C., Malafarina, D., & Modesto, L. 2013, *Phys. Rev. D*, 88, 044409
- Bambi, C., & Yoshida, N. 2010, *Classical and Quantum Gravity*, 27, 205006
- Barausse, E., & Sotiriou, T. P. 2008, *Physical Review Letters*, 101, 099001
- Bélanger, G., Terrier, R., de Jager, O. C., Goldwurm, A., & Melia, F. 2006, *Journal of Physics Conference Series*, 54, 420
- Broderick, A. E., & Loeb, A. 2005, *MNRAS*, 363, 353
- Broderick, A. E., & Loeb, A. 2006, *MNRAS*, 367, 905
- Broderick, A. E., Loeb, A., & Narayan, R. 2009, *ApJ*, 701, 1357
- De Villiers, J.-P., Hawley, J. F., & Krolik, J. H. 2003, *ApJ*, 599, 1238
- Do, T., Ghez, A. M., Morris, M. R., et al. 2009, *ApJ*, 691, 1021
- Dodds-Eden, K., Gillessen, S., Fritz, T. K., et al. 2011, *ApJ*, 728, 37
- Dodds-Eden, K., Sharma, P., Quataert, E., et al. 2010, *ApJ*, 725, 450
- Doeleman, S., Agol, E., Backer, D., et al. 2009, *astro2010: The Astronomy and Astrophysics Decadal Survey*, 2010, 68
- Doeleman, S. S., Weintroub, J., Rogers, A. E. E., et al. 2008, *Nature*, 455, 78
- Drappeau, S., Dibi, S., Dexter, J., Markoff, S., & Fragile, P. C. 2013, *MNRAS*, 431, 2872
- Eckart, A., Baganoff, F. K., Morris, M., et al. 2004, *A&A*, 427, 1
- Eckart, A., Baganoff, F. K., Morris, M. R., et al. 2009, *A&A*, 500, 935
- Eisenhauer, F., Perrin, G., Brandner, W., et al. 2008, *Proc. SPIE*, 7013E, 69
- Eisenhauer, F., Perrin, G., Brandner, W., et al. 2011, *The Messenger*, 143, 16
- Fabian, A. C., Rees, M. J., Stella, L., & White, N. E. 1989, *MNRAS*, 238, 729
- Falcke, H., & Markoff, S. B. 2013, *Classical and Quantum Gravity*, 30, 244003
- Falcke, H., Melia, F., & Agol, E. 2000, *ApJ*, 528, L13
- Genzel, R., Eisenhauer, F., & Gillessen, S. 2010, *Reviews of Modern Physics*, 82, 3121
- Genzel, R., Schödel, R., Ott, T., et al. 2003, *Nature*, 425, 934
- Ghez, A. M., Wright, S. A., Matthews, K., et al. 2004, *ApJ*, 601, L159
- Hamaus, N., Paumard, T., Müller, T., et al. 2009, *ApJ*, 692, 902

- Johannsen, T., & Psaltis, D. 2010, *ApJ*, 718, 446
 Johannsen, T., & Psaltis, D. 2011a, *ApJ*, 726, 11
 Johannsen, T., & Psaltis, D. 2011b, *Phys. Rev. D*, 83, 124015
 Johannsen, T., & Psaltis, D. 2013, *ApJ*, 773, 57
 Joshi, P. S., Malafarina, D., & Narayan, R. 2014, *Classical and Quantum Gravity*, 31, 015002
 Kalogera, V., & Baym, G. 1996, *ApJ*, 470, L61
 Krawczynski, H. 2012, *ApJ*, 754, 133
 Li, L.-X., Zimmerman, E. R., Narayan, R., & McClintock, J. E. 2005, *ApJS*, 157, 335
 Li, Y.-R., Wang, J.-M., & Ho, L. C. 2012, *ApJ*, 749, 187
 Li, Z., & Bambi, C. 2013, *J. Cosmol. Astropart. Phys.*, 3, 31
 Li, Z., & Bambi, C. 2014, *J. Cosmol. Astropart. Phys.*, 1, 41
 Liu, K., Wex, N., Kramer, M., Cordes, J. M., & Lazio, T. J. W. 2012, *ApJ*, 747, 1
 Lund, E., Bugge, L., Gavrilenko, I., & Strandlie, A. 2009, *JINST*, 4, P04001
 Maoz, E. 1998, *ApJ*, 494, L181
 Markoff, S., Falcke, H., Yuan, F., & Biermann, P. L. 2001, *A&A*, 379, L13
 McClintock, J. E., Narayan, R., & Steiner, J. F. 2013, *Space Sci. Rev.*, 73
 Narayan, R., & Heyl, J. S. 2002, *ApJ*, 574, L139
 Narayan, R., & McClintock, J. E. 2008, *New Astronomical Review*, 51, 733
 Narayan, R., & McClintock, J. E. 2012, *MNRAS*, 419, L69
 Psaltis, D., Perrodin, D., Dienes, K. R., & Mocioiu, I. 2008, *Physical Review Letters*, 100, 119902
 Remillard, R. A., Muno, M. P., McClintock, J. E., & Orosz, J. A. 2002, *ApJ*, 580, 1030
 Rhoades, C. E., & Ruffini, R. 1974, *Physical Review Letters*, 32, 324
 Schnittman, J. D. 2005, *ApJ*, 621, 940
 Schnittman, J. D. 2006, Ph.D. Thesis
 Schnittman, J. D., & Bertschinger, E. 2004, *ApJ*, 606, 1098
 Schnittman, J. D., Krolik, J. H., & Hawley, J. F. 2006, *ApJ*, 651, 1031
 Stella, L., & Vietri, M. 1998, *ApJ*, 492, L59
 Stella, L., & Vietri, M. 1999, *Physical Review Letters*, 82, 17
 Tagger, M., & Melia, F. 2006, *ApJ*, 636, L33
 Takahashi, R. 2004, *ApJ*, 611, 996
 Trap, G., Goldwurm, A., Dodds-Eden, K., et al. 2011, *A&A*, 528, A140
 Trippe, S., Paumard, T., Ott, T., et al. 2007, *MNRAS*, 375, 764
 Tsukamoto, N., Li, Z., & Bambi, C. 2014, arXiv:1403.0371
 Vincent, F. H., Paumard, T., Perrin, G., et al. 2011, *MNRAS*, 412, 2653
 Wei, S.-W., & Liu, Y.-X. 2013, *J. Cosmol. Astropart. Phys.*, 11, 63
 Wex, N., & Kopeikin, S. M. 1999, *ApJ*, 514, 388
 Yusef-Zadeh, F., Roberts, D., Wardle, M., Heinke, C. O., & Bower, G. C. 2006, *ApJ*, 650, 189
 Zhang, S. N., Cui, W., & Chen, W. 1997, *ApJ*, 482, L155